Comb-Referenced Doppler-Free Spectrometry of the ^{200}Hg and ^{202}Hg Intercombination Line at 254 nm

Stefania Gravina[⬛],[1] Naveed A. Chishti[⬛],[1] Simona Di Bernardo[⬛],[1] Eugenio Fasci[⬛],[1] Antonio Castrillo[⬛],[1]
Athanasios Laliotis[⬛],[2] and Livio Gianfrani[⬛][1,*]

[1]*Dipartimento di Matematica e Fisica, Università degli Studi della Campania "Luigi Vanvitelli", 81100 Caserta, Italy*
[2]*Laboratoire de Physique des Lasers, Université Sorbonne Paris Nord, 93430 Villetaneuse, France*

We report on precision spectroscopy of the $6s^2\ ^1S_0 \to 6s6p\ ^3P_1$ intercombination line of mercury in the deep ultraviolet, by means of a frequency-comb referenced, wavelength-modulated, saturated absorption technique. This method allowed us to perform sub-Doppler investigations with an absolute frequency axis at 254 nm, while ensuring a relatively high signal-to-noise ratio. The absolute line center frequencies of the ^{200}Hg and ^{202}Hg bosonic isotopes were measured with a global uncertainty of 8 and 15 kHz (namely, 6.8×10^{-12} and 1.3×10^{-11}, in relative terms), respectively, the statistical and systematic components being significantly reduced as compared to past determinations. This remarkable result was achieved also thanks to an in-depth study of the ac Stark effect. Furthermore, we found the most accurate ^{200}Hg-^{202}Hg isotope shift ever obtained before, namely, $5\,295\,57\,0 \pm 15_{\text{stat}} \pm 8_{\text{syst}}$ kHz.

In recent years, renewed interest has emerged in the isotopic shift of atomic transitions. In fact, isotope shift spectroscopy in heavy atoms can be used to look for new forces beyond the standard model, as well as to determine basic properties of atomic nuclei [1]. More particularly, when collecting spectroscopic data on at least four isotopes, it is possible to constrain new physics scenarios by testing very accurately the linearity of King plots [2]. The King plot analysis was extensively used in the 1980s and 1990s to investigate the field shift, which originates from the different nuclear volumes of the various isotopes of a given element [3–5]. Nevertheless, there might be nonlinear corrections to the King plots that can be justified already in the standard model framework. This is the case of the nuclear polarizability contribution, which can lead to a significant deviation from linearity. Very recently, the clear nonlinearity in the joint Yb/Yb$^+$ King-plot analysis has been mostly accounted for by the deformation of the Yb nuclei [6,7]. In this regard, it has been argued that a direct comparison between theory and experiment on a single transition for a single pair of isotopes can yield more stringent bounds with the same amount of theoretical effort [8].

A few years ago, absolute center frequencies and isotope shifts were determined for the Hg $6s^2\ ^1S_0 \to 6s6p\ ^3P_1$ line with an accuracy of a few hundred kHz, namely, more than 1 order of magnitude better than any previous measurement [9]. With its seven stable isotopes, four of which having zero nuclear spin (^{198}Hg, ^{200}Hg, ^{202}Hg, and ^{204}Hg), mercury is a quite interesting atom for fundamental tests and measurements [10]. It is a good candidate for the development of a primary frequency reference, due to some favorable characteristics, such as its sensitivity to blackbody radiation, which is lower than that of Sr and Yb [11]. The intercombination transition plays a key role in the search for a permanent electric dipole moment in the $^1S_0$ electronic ground state of the ^{199}Hg atom, the spectral line being involved in a pump-probe process based upon spin polarization [12]. As for many transitions from the ground state ns^2 to the $nsnp$ configurations of two-electron atoms or ions, the Hg intercombination line is a highly sensitive probe of possible long-term variations of the fine-structure constant [13]. An ongoing experiment in Caserta employs the Hg intercombination line at 253.7 nm for temperature metrology, by using comb-calibrated Doppler width spectrometry [14,15]. This latter is a promising primary method for the practical realization of the new kelvin definition, which is in force since 20 May 2019 [16]. In this technique, once the Doppler width is retrieved from the precise observation of the absorption line shape in a gas at the thermodynamic equilibrium, the absolute temperature can be determined by inverting the well-known expression of the Doppler width, provided that the line center frequency is accurately known [17].

In this framework, the present Letter has a twofold objective: to measure the center frequency of the Hg intercombination line at the precision level of 10 kHz; to improve significantly the current knowledge of the ^{200}Hg-^{202}Hg isotope shift of this spectral line. To pursue these goals, we developed a rather advanced apparatus capable of Doppler-free precision spectroscopic measurements with a wavelength-modulation (WM) technique, by
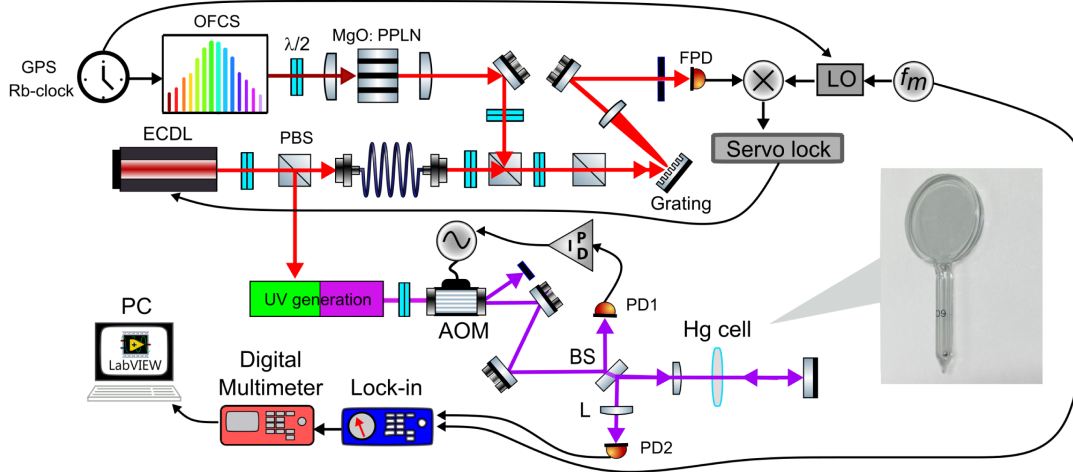
FIG. 1. Sketch of the experimental setup. External-cavity diode laser (ECDL); optical frequency comb synthesizer (OFCS); periodically poled MgO-doped LiNbO$_3$ crystal (MgO:PPLN); photodiode (PD); fast photodiode (FPD); local oscillator (LO); polarizing beam splitter (PBS); 50% beam splitter (BS); plano-convex lens (L).

using low-power coherent radiation in the deep-ultraviolet region. The spectrometer is schematically depicted in Fig. 1. As extensively described in Refs. [14,18], the laser source consists of a double-stage duplication of a 1014.8 nm ECDL. After spatial filtering by means of a 200-μm pinhole, the UV radiation at the wavelength of 253.7 nm passes through an acousto-optic modulator (AOM), which has a twofold function: first, it is used to finely change the UV power of the zero order that is used for the spectroscopic experiment; second, it is the actuator of an intensity control feedback loop, thereby stabilizing the UV power at the level of one part in 10^4 within a few tens of minutes, in the baseband region. To this aim, a portion of the UV beam is monitored by a first silicon carbide (SiC) photodetector. The remaining portion of the UV radiation (whose power can go up to ∼10 μW, depending on the radio-frequency power driving the AOM) is directed towards a 1-mm-long mercury vapor cell. Sealed at the two ends by a pair of Spectrosil far-UV quartz windows, the cell has a cylindrical geometry with a 2-cm diameter and it is equipped with a small reservoir in the middle of its length. As guaranteed by the manufacturer (Precision Glassblowing Inc.), the cell is baked at 425 °C for a minimum of 24 h in an ultrahigh vacuum environment prior to any introduction of mercury in the reservoir. This process ensures ultrapure Hg vapors in equilibrium with the liquid phase inside the cell. The reservoir is immersed into a homemade liquid-bath thermostat based on Peltier cells, whose temperature can be adjusted from 0 °C to 50 °C. So doing, it is possible to tune the vapor pressure in the thin cell roughly from 2×10^{-2} to 2 Pa.

We implemented the conventional pump-probe scheme in which the traveling laser beam, after passing through the thin cell, is retroreflected towards the cell by a plane mirror. To ensure the precise alignment and overlap of the two beams, a pair of pinholes are positioned along the beam

path. Care was taken to gently focus the pump beam in the center of the cell. The reflected probe beam returns to the beam splitter and subsequently is focused on a second SiC photodetector.

The near-infrared ECDL is tightly locked to an optical frequency comb synthesizer (MENLO Systems, FC1500-250-WG) based on a mode-locked, femtosecond, erbium-doped fiber laser at 1560 nm and stabilized against a GPS-disciplined Rb clock. Details are provided in the Supplemental Material [19]. The absolute UV frequency can be easily retrieved from the following equation:

$$f_{\text{UV}} = 4 \times (f_{\text{beat}} + m f_{\text{rep}} + 2 f_{\text{ceo}}), \tag{1}$$

where f_{beat} is the beat note frequency at 1015 nm, m is the comb tooth order, f_{rep} and f_{ceo} are the comb repetition rate (= 250 MHz) and the carrier-envelope offset frequency (= 20 MHz), respectively. The comb order was unambiguously determined by measuring the ECDL wavelength in the near-infrared with a 9-digit wave meter.

High sensitivity detection of the relatively small Lamb-dip was achieved by using a WM technique, which is inspired by the developments of Gambetta *et al.* in the field of midinfrared frequency-comb referenced molecular spectroscopy [20]. To this aim, the LO frequency is dithered at $f_m = 220$ Hz. Thanks to the action of the locking loop, the sinusoidal modulation is effectively transferred to the ECDL frequency and, consequently, to the UV radiation so as to set the modulation index to about 1. An analog lock-in amplifier was used to perform the first-harmonic synchronous detection of the probe beam intensity, thus leading to a dispersive signal in coincidence with the Lamb dip. Calibrated frequency scans across the intercombination line were obtained by finely tuning the f_{rep} frequency while the ECDL was locked to the comb. A $6\frac{1}{2}$-digit voltmeter,
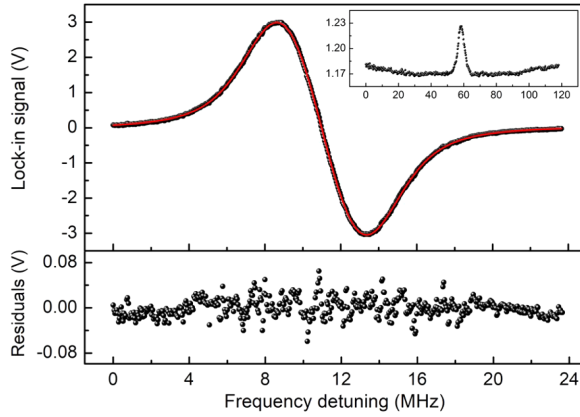
FIG. 2. The top panel shows the dispersive ^{200}Hg sub-Doppler spectrum, as obtained by means of the wavelength-modulated technique at a vapor pressure of ∼0.24 Pa. For comparison, an example of Lamb-dip spectrum is reported in the inset. The red line represents the best-fit curve, while the bottom plot gives the residuals. The SNR amounts to ∼370. The saturation intensity was calculated to be ∼110 mW/cm^2, while the UV radiation intensity in the beam waist was ∼15 mW/cm^2.
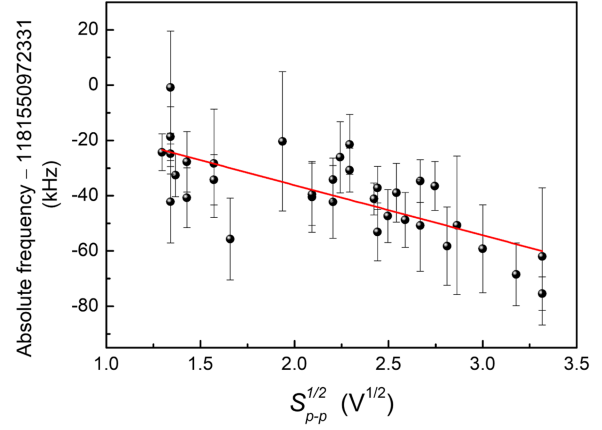

FIG. 3. Line centers as a function of the square root of the peak-to-peak signal. Each point is the mean value of the center frequencies from two consecutive scans at a certain UV power. Vertical bars result from error propagation of line fitting uncertainties and subsequent multiplication by a factor of 3. This is done in order to be very prudent in quoting the statistical uncertainty of the retrieved parameters. The red solid line is the weighted linear fit of the data.

connected to a personal computer, is used for spectral acquisitions, as governed by a LabVIEW code that also controls f_{rep}.

An example of sub-Doppler spectrum for the ^{200}Hg $6s^2$ $^1S_0 \rightarrow 6s6p\ ^3P_1$ transition is shown in Fig. 2. Compared to direct detection of absorption, which leads to Lamb-dip spectra similar to the one shown in the inset of Fig. 2, the WM technique ensures background flattening in conjunction to a higher signal-to-noise ratio (SNR), circumstance that allows one to retrieve the line center frequency more accurately. This spectrum consists of 500 points that are acquired in 73 s. We operate in the weak saturation regime, the Lamb-dip contrast ranging between 3% and 5%, while the single-pass linear absorption amounts to ∼54%. A refined line fitting is a key factor to accurately retrieve the absolute center frequency. It is well known that wavelength modulation leads to lock-in signals that are proportional to various Fourier coefficients of the modulated line shape function, depending on the order of the harmonic that is detected. We adopted as a line shape model the wavelength-modulated Voigt function, as described in Ref. [21]. Details about the line shape model are provided in the Supplemental Material [19]. Fit residuals exhibit a root-mean-square value of about 16 mV, thus demonstrating the excellent agreement between the experimental data and the line shape model, as shown in the bottom plot of Fig. 2. The spectral analysis gives a full width at half maximum (FWHM) of the sub-Doppler line of about 5 MHz, which includes the natural width of the line ($\approx$1.3 MHz), Zeeman and collisional broadening, as well as the transit-time broadening ($\approx$320 kHz). It is worth noting that the observed width is close to the expected one ($\approx$ 6 MHz).

The slight discrepancy is probably due to an overestimation of the calculated Zeeman broadening effect.

The experimental strategy is to retrieve one center frequency value from a pair of round-trip scans, to cancel out the frequency shifts induced by the limited detection bandwidth [22,23]. Additional information on this effect is provided in the Appendix. Moreover, Lamb-dip measurements were repeated as a function of the incident UV power to take into account the possible occurrence of the ac Stark shift. In our experiment, the UV power hitting the cell was varied from 1 up to 10 µW, which gives an intensity in the beam waist, I_0, approximately between 3 and 30 mW/cm^2. These values were determined by using a UV beam profiler in conjunction to a calibrated SiC photodiode. In Fig. 3, we report the results of this investigation for the ^{200}Hg isotope. The center frequencies are plotted as a function of the square root of the peak-to-peak signal, S_{p-p}. This latter can be retrieved from the fit of wavelength-modulated sub-Doppler spectra. Furthermore, S_{p-p} is proportional to the Lamb-dip amplitude, which in turn increases with I_0^2, in the weak saturation regime. Figure 3 shows that our measurements are clearly affected by a negative ac Stark shift. A linear regression of the data gives the zero-intensity center frequency, equal to 1 181 550 972 331(6) kHz, the reported uncertainty being of pure statistical nature at 1σ. The measurement procedure was also applied to the ^{202}Hg line, resulting in an absolute center frequency of 1 181 545 676 761(14) kHz. After proper calibration of the peak-to-peak signal, the ac Stark effect was quoted to be -2.8 ± 0.5 and -2.2 ± 0.8 kHz/mW/cm^2, respectively, for ^{200}Hg and ^{202}Hg. The former differs significantly from the estimate of Ref. [9], while the latter is in good agreement. It should

TABLE I. Uncertainty budget related to the line center frequency measurements for the ^{200}Hg and ^{202}Hg isotopes.

Contribution	Type A (kHz)	Type B (kHz)
Statistical uncertainty	6–14	
Frequency calibration		3
Pressure shift		5
2nd-order Doppler shift		<0.2
Overall combined uncertainty	8–15	

be noted that, in the two-level atom approximation, no frequency shift is expected from the resonant UV radiation. Nevertheless, light shift contributions can originate by other electric-dipole transitions involving one of the two states of the intercombination transition, whose frequencies are close to the incident UV radiation. Using time-dependent second-order perturbation theory, energy shifts due to nonresonant light can be estimated [24]. We found that the shift of the intercombination line is mostly due to the negative energy shift of the $6s6p$ $^3P_1$ state, this latter showing a strong dipole coupling with highly excited states, including $6s9s$ $^3S_1$ and $6s8d$ $^3D_{0,1,2}$.

Table I presents the complete uncertainty budget. The OFCS contributes with an uncertainty of ∼3 kHz, arising from the stability of the GPS-disciplined Rb clock, which amounts to 2.5×10^{-12} at 1 s. We quantified the contribution of the pressure shift, also taking into account residual gases that may form in the sealed cell, namely, helium, water, and molecular hydrogen. Diffusion from ambient air may lead to a He partial pressure into the quartz cell of up to ∼0.5 Pa. From the pressure shifting coefficient due to He-Hg collisions, as reported in Ref. [25], we retrieved an upper limit to the shift of +5 kHz. Instead, the estimated coefficient of the Hg-Hg collision-induced frequency shift results to be −22 kHz/Pa, in sub-Doppler experiments [9]. This latter produces a negative shift of −5.3 kHz. As for the other gases, H_2O and H_2, we expect partial pressures much smaller than 1 Pa, due to the cell manufacturing process. This is confirmed by the relatively narrow Lamb dips that are observed. Since the joint effect of the various collision partners partially cancels out, a conservative estimate of the uncertainty contribution coming from the overall pressure shift can be 5 kHz at 1σ. The 2nd-order Doppler shift was quoted to be about −160 Hz. The recoil effect in the case of two counterpropagating beams leads to a doublet whose frequency separation is ∼30 kHz, namely, much smaller that the width of the sub-Doppler feature. Because of its symmetry, the unresolved doublet is not expected to produce a shift of the center frequency [26]. Similarly, possible shifts resulting from Zeeman, gas lens, and wavefront-curvature-induced residual Doppler effects are negligible. The overall uncertainties are quoted to be 8 and 15 kHz, respectively, for

^{200}Hg and ^{202}Hg. Consequently, the level of knowledge is improved by more than a factor of 20 for ^{200}Hg and a factor of 7 for ^{202}Hg, compared to the most recent determinations [9]. From the absolute frequency measurements given above, it is possible to determine the shift between the ^{200}Hg and ^{202}Hg isotopes, which amounts to $5\,295\,570 \pm 15_{stat} \pm 8_{syst}$ kHz. Our determination should be compared with the one resulting from the data of Ref. [9], namely, $5\,295\,413 \pm 110_{stat} \pm 180_{syst}$ kHz. The two values agree satisfactorily, their difference being 157 kHz.

In conclusion, we have improved significantly the current knowledge of the absolute frequency of the mercury intercombination line in the deep-UV, using comb-locked wavelength-modulated saturated absorption spectroscopy, a powerful technique that allowed us to achieve a relative precision of 6.8×10^{-12} and 1.3×10^{-11}, respectively, for the ^{200}Hg and ^{202}Hg isotopes. As a result, the ^{200}Hg-^{202}Hg isotope shift could be measured more precisely and accurately, the statistical and systematical uncertainties being reduced by a factor of ∼7 and ∼23, respectively, compared to the recent experiment of Ref. [9]. It would be interesting to make a comparison with accurate theoretical calculations. In this regard, our study can stimulate the extension to Hg isotopes of relativistic multiconfiguration Dirac-Hartree-Fock calculations, recently performed for the ytterbium intercombination line [27], thus paving the way to experimental and theoretical investigations of quantum electrodynamics and nuclear size effects in Hg atoms for testing fundamental physical theories. Furthermore, the application of our method to ultrathin Hg cells of sub-μm thickness would provide the possibility to look for Casimir-Polder interactions with a non-hydrogen-like atom or study atom-wall collisions in mercury vapors.

Appendix: The finite bandwidth effect.—Figure 4 shows the results obtained from the spectral analysis of 10 repeated acquisitions of the sub-Doppler feature at the liquid mercury temperature of 24 °C, with an incident power of ∼9 μW. The line center frequencies that are retrieved from scans with a positive sweep speed, $\dot{\nu} = d\nu/dt$, are clearly shifted with respect to those resulting from scans with $\dot{\nu} < 0$. The former data are labeled in Fig. 4 with odd acquisition numbers, while the latter present an even acquisition index. This is a systematic deviation that is due to the finite bandwidth of the detection electronics with which spectra are recorded, an effect that is often underestimated [22]. It is worth noting that the effect is clearly measurable despite the fact that no line asymmetry is observed. The sub-Doppler spectra are acquired with a sweep speed of
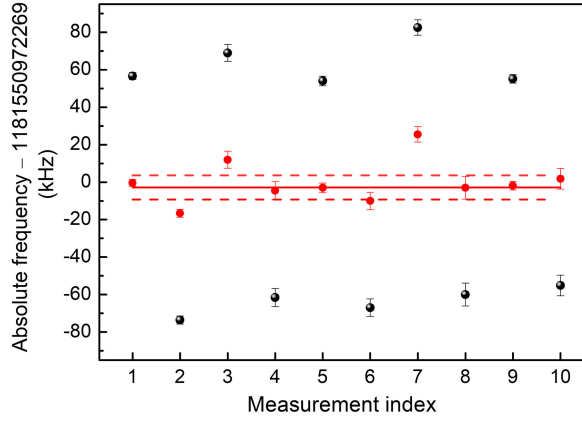
FIG. 4. Finite bandwidth effect. Absolute line center frequencies for the ^{200}Hg isotope at 24 °C are shown as black points. The red points are the corrected frequencies.

± 0.326 MHz/s and a lock-in amplifier time constant, τ_D, of 100 ms. Each frequency step, $\Delta\nu$, has a time duration, Δt, of 145 ms. The lock-in amplifier, operating in the -12 dB/octave roll-off mode, can be conceptualized as two consecutive first-order filters with identical characteristics [22]. In this mode of operation, the filter quality factor is equal to $1/2$. According to the description of Ref. [23], which applies to a step-by-step frequency-sweeping mode, it is possible to define a frequency constant given by $\nu_D = \theta\Delta\nu$, θ being the ratio $\tau_D/\Delta t$ that is equal to ~ 0.66 in our operation conditions. It is found that the retrieved center frequency, denoted as ν_{0fit}, deviates from the true value according to the equation [23]

$$\nu_{0\text{fit}} - \nu_0 = \frac{\exp\left(-\frac{1-2\eta}{2\theta}\right)}{\sinh\left(\frac{1}{2\theta}\right)} \times A \times \Delta\nu/2, \qquad (A1)$$

where η is the dead-time constant that is defined as $(\Delta t - \Delta t_a)/\Delta t$, namely, the ratio between the technical dead time occurring between signal acquisition (over a time span Δt_a) and next frequency change and the step duration. The quantity A is a function of η and θ, defined as follows:

$$A(\eta, \theta) = 1 + \frac{1-2\eta}{2\theta} + \frac{1}{2\theta}\coth\left(\frac{1}{2\theta}\right). \qquad (A2)$$

Since the dead time for each frequency step is ~ 50 ms, the frequency shift amounts to ± 57 kHz (depending on the sign of $\Delta\nu$), which is in good agreement with the observed systematic deviations. Therefore, as a side result of our work, we can confirm the validity of the model of Ref. [23], as demonstrated by the red points of Fig. 4, for which the frequency shift has been removed. Here, the zero of the vertical scale is set in coincidence with the mean value of the uncorrected frequencies

(black points), while the solid red line gives the weighted mean of the corrected frequencies (red points), the dashed-dotted lines representing the 2σ confidence interval. We used the corrected uncertainty on the weighted mean as a result of a mutual consistency test, thus following the recommendations of the *Bureau International des Poids et Mesures* (BIPM) [28]. The mean value falls well within this range. On the other hand, Eq. (A1) tells us that the systematic deviations cancel out if we take the mean value of the center frequencies resulting from two consecutive scans, the former characterized by $\Delta\nu > 0$, the latter with $\Delta\nu < 0$. This is the reason why it is essential to obtain the center frequency value from two consecutive scans.

[1] C. Frugiuele, E. Fuchs, G. Perez, and M. Schlaffer, Constraining new physics models with isotope shift spectroscopy, Phys. Rev. D **96**, 015011 (2017).

[2] V. V. Flambaum, A. J. Geddes, and A. V. Viatkina, Isotope shift, nonlinearity of King plots, and the search for new particles, Phys. Rev. A **97**, 032510 (2018).

[3] W. H. King, *Isotope Shifts in Atomic Spectra* (Springer Science & Business Media, New York, 2013).

[4] M. D. Rayman, C. G. Aminoff, and J. L. Hall, Precise laser frequency scanning using frequency-synthesized optical frequency sidebands: Application to isotope shifts and hyperfine structure of mercury, J. Opt. Soc. Am. B **6**, 539 (1989).

[5] L. Gianfrani, A. Sasso, G. M. Tino, and M. Inguscio, Experimental indication of a nuclear volume contribution to the isotope shift of atomic oxygen, Opt. Commun. **78**, 158 (1990).

[6] N. L. Figueroa, J. C. Berengut, V. A. Dzuba, V. V. Flambaum, D. Budker, and D. Antypas, Precision determination of isotope shifts in ytterbium and implications for new physics, Phys. Rev. Lett. **128**, 073001 (2022).

[7] J. Hur, D. P. L. Aude Craik, I. Counts, E. Knyazev, L. Caldwell, C. Leung, S. Pandey, J. C. Berengut, A. Geddes, W. Nazarewicz, P.-G. Reinhard, A. Kawasaki, H. Jeon, W. Jhe, and V. Vuletić, Evidence of two-source King plot nonlinearity in spectroscopic search for new boson, Phys. Rev. Lett. **128**, 163201 (2022).

[8] V. Debierre, N. S. Oreshkina, I. A. Valuev, Z. Harman, and C. H. Keitel, Testing standard-model extensions with isotope shifts in few-electron ions, Phys. Rev. A **106**, 062801 (2022).

[9] M. Witkowski, G. Kowzan, R. Munoz-Rodriguez, R. Ciuryło, P. S. Żuchowski, P. Masłowski, and M. Zawada, Absolute frequency and isotope shift measurements of mercury $^1S_0 - ^3P_1$ transition, Opt. Express **27**, 11069 (2019).

[10] M. S. Safronova, D. Budker, D. DeMille, D. F. J. Kimball, A. Derevianko, and C. W. Clark, Search for new physics with atoms and molecules, Rev. Mod. Phys. **90**, 025008 (2018).

[11] J. J. McFerran, L. Yi, S. Mejri, S. Di Manno, W. Zhang, J. Guéna, Y. Le Coq, and S. Bize, Neutral atom frequency

reference in the deep ultraviolet with fractional uncertainty $=$ 5.7×10^{-15}, Phys. Rev. Lett. **108**, 183004 (2012).

[12] B. Graner, Y. Chen, E. G. Lindahl, and B. R. Heckel, Reduced limit on the permanent electric dipole moment of ^{199}Hg, Phys. Rev. Lett. **116**, 161601 (2016).

[13] E. J. Angstmann, V. A. Dzuba, and V. V. Flambaum, Relativistic effects in two valence-electron atoms and ions and the search for variation of the fine-structure constant, Phys. Rev. A **70**, 014102 (2004).

[14] C. Clivati, S. Gravina, A. Castrillo, G. A. Costanzo, F. Levi, and L. Gianfrani, Tunable UV spectrometer for Doppler broadening thermometry of mercury, Opt. Lett. **45**, 3693 (2020).

[15] S. Gravina, C. Clivati, N. A. Chishti, A. Castrillo, E. Fasci, F. Bertiglia, G. Lopardo, A. Sorgi, N. Coluccelli, G. Galzerano, P. C. Pastor, F. Levi, and L. Gianfrani, Comb-assisted mercury spectroscopy in the deep-ultraviolet: Towards the development of a new primary thermometer, J. Phys. Conf. Ser. **2439**, 012015 (2023).

[16] G. Machin, The kelvin redefined, Meas. Sci. Technol. **29**, 022001 (2018).

[17] L. Gianfrani, Linking the thermodynamic temperature to an optical frequency: Recent advances in Doppler broadening thermometry, Phil. Trans. R. Soc. A **374**, 20150047 (2016).

[18] S. Gravina, C. Clivati, A. Castrillo, E. Fasci, N. A. Chishti, G. Galzerano, F. Levi, and L. Gianfrani, Measurement of the mercury (6s6p) ^{3}P$_1$-state lifetime in the frequency domain from integrated absorbance data, Phys. Rev. Res. **4**, 033240 (2022).

[19] See Supplemental Material at http://link.aps.org/supplemental/10.1103/PhysRevLett.132.213001 for the comb-locking approach and the lineshape model.

[20] A. Gambetta, E. Vicentini, N. Coluccelli, Y. Wang, T. T. Fernandez, P. Maddaloni, P. De Natale, A. Castrillo, L. Gianfrani, P. Laporta, and G. Galzerano, Versatile mid-infrared frequency-comb referenced sub-Doppler spectrometer, APL Photonics **3**, 046103 (2018).

[21] J. Westberg, J. Wang, and O. Axner, Fast and non-approximate methodology for calculation of wavelength-modulated Voigt lineshape functions suitable for real-time curve fitting, J. Quant. Spectrosc. Radiat. Transfer **113**, 2049 (2012).

[22] F. Rohart, S. Mejri, P. L. T. Sow, S. K. Tokunaga, C. Chardonnet, B. Darquié, H. Dinesan, E. Fasci, A. Castrillo, L. Gianfrani *et al.*, Absorption-line-shape recovery beyond the detection-bandwidth limit: Application to the precision spectroscopic measurement of the Boltzmann constant, Phys. Rev. A **90**, 042506 (2014).

[23] F. Rohart, Overcoming the detection bandwidth limit in precision spectroscopy: The analytical apparatus function for a stepped frequency scan, J. Quant. Spectrosc. Radiat. Transfer **187**, 490 (2017).

[24] J. E. Stalnaker, D. Budker, S. J. Freedman, J. S. Guzman, S. M. Rochester, and V. V. Yashchuk, Dynamic stark effect and forbidden-transition spectral line shapes, Phys. Rev. A **73**, 043416 (2006).

[25] E. Lewis, Collisional relaxation of atomic excited states, line broadening and interatomic interactions, Phys. Rep. **58**, 1 (1980).

[26] M. Petersen, R. Chicireanu, S. T. Dawkins, D. V. Magalhães, C. Mandache, Y. Le Coq, A. Clairon, and S. Bize, Doppler-free spectroscopy of the $^1S_0 - ^3P_0$ optical clock transition in laser-cooled fermionic isotopes of neutral mercury, Phys. Rev. Lett. **101**, 183004 (2008).

[27] J. S. Schelfhout and J. J. McFerran, Isotope shifts for $^1S_0 - ^3P^o_{0,1}$ Yb lines from multiconfiguration Dirac-Hartree-Fock calculations, Phys. Rev. A **104**, 022806 (2021).

[28] Bureau International des Poids et Mesures (BIPM), Estimation of a consensus KCRV and associated degrees of equivalence, CCQM Guidance note https://www.bipm.org/documents/20126/28430045/working-document-ID-5794/49d366bc-295f-18ca-c4d3-d68aa54077b5 (2013).